Wetland characterization using polarimetric RADARSAT-2 capability

R. Touzi, A. Deschamps, and G. Rother

Abstract. The use of single-polarization (HH) RADARSAT-1 synthetic aperture radar (SAR) data has been shown to be important for wetland water extent characterization. However, the limited capability of the RADARSAT-1 single-polarization C-band SAR in vegetation type discrimination makes the use of clear-sky-dependent visible near-infrared (VNIR) satellite data necessary for wetland mapping. In this paper, the potential of polarimetric RADARSAT-2 data for wetland characterization is investigated. The Touzi incoherent decomposition is applied for the roll-invariant decomposition of wetland scattering. In contrast with the Cloude–Pottier decomposition that characterizes target scattering type with a real entity, α, the Touzi decomposition uses a complex entity, the symmetric scattering type, for unambiguous characterization of wetland target scattering. It is shown that, like the Cloude α scattering type, the magnitude α_s of the symmetric scattering is not effective for vegetation type discrimination. The phase ϕ_{α_s} of the symmetric scattering type has to be used for better characterization of wetland vegetation species. The unique information provided by ϕ_{α_s} for an improved wetland class discrimination is demonstrated using Convair-580 polarimetric C-band SAR data collected over the Mer Bleue wetland in the east of Ottawa, Canada. The use of ϕ_{α_s} makes possible the discrimination of shrub bog from sedge fen and even permits the discrimination between conifer-dominated treed bog and upland deciduous forest under leafy conditions.

Résumé. L'utilisation des données radar à synthèse d'ouverture (RSO) de RADARSAT-1 en polarisation unique (HH) a déjà fait ses preuves pour la caractérisation de l'étendue d'eau en milieu humide. Cependant, la capacité limitée du RSO en bande C de RADARSAT-1 en polarisation unique pour la détermination des types de végétation rend nécessaire l'utilisation de données satellitaires dans le proche infrarouge visible (VNIR) qui sont dépendantes de conditions de ciel clair pour la cartographie des milieux humides. Dans cet article, nous analysons le potentiel des données polarimétriques de RADARSAT-2 pour la caractérisation des milieux humides. La décomposition incohérente de Touzi est utilisée pour la décomposition invariante du signal radar diffusé par les milieux humides. Par opposition à la décomposition Cloude–Pottier qui caractérise le type de diffusion de cible par le biais d'une entité réelle, α, la décomposition de Touzi utilise une entité complexe, de type diffusion symétrique, pour la caractérisation sans ambiguïté de la diffusion de cible en milieu humide. Il est démontré que, comme pour la diffusion de type Cloude α, l'amplitude α_s de la diffusion symétrique n'est pas efficace pour la détermination des types de végétation. La phase ϕ_{α_s} de la diffusion symétrique doit être utilisée pour une meilleure caractérisation des espèces en milieu humide. L'information inédite apportée par ϕ_{α_s} au plan de l'amélioration de la discrimination des classes en milieu humide est démontrée à l'aide de données polarimétriques RSO en bande C du Convair-580 acquises au-dessus de la tourbière de la Mer Bleue, à l'est d'Ottawa, au Canada. L'utilisation de ϕ_{α_s} rend possible la distinction des tourbières arbustives par rapport aux fen et permet même de distinguer entre les tourbières boisées dominées par les conifères et les forêts de feuillus des hautes terres sous conditions de feuillage.

Introduction

Wetlands play a key role in regional and global environments and are critically linked to major issues such as climate change, water quality, the hydrological and carbon cycles, and wildlife habitat and biodiversity. Their existence is crucial to maintaining a balanced hydrological system, and wetlands act as indicators of environment health. Mapping wetlands and monitoring their change in a systematic and repeatable manner for the Canadian Wetland Inventory (CWI) (Helie, 2004) are important to manage and protect significant wetland areas in

Canada. The use of RADARSAT-1 synthetic aperture radar (SAR) data has been shown to be important for wetland water extent characterization (Toyra et al., 2001; Grenier et al., 2005; Li and Chen, 2005). However, the limited capability of the RADARSAT-1 single-polarization C-band SAR in vegetation type discrimination makes the use of clear-sky-dependent visible near-infrared (VNIR) satellite data necessary for wetland mapping (Helie, 2004; Toyra et al., 2001; Toyra and Pietroniro, 2005; Grenier et al., 2005; Li and Chen, 2005). Hence, the CWI is being completed using a combination of

R. Touzi[1] and A. Deschamps. Canada Centre for Remote Sensing, Natural Resources Canada, 588 Booth Street, Ottawa, ON K1A 0Y7, Canada.

G. Rother. National Capital Commission, 40 Elgin Street, Ottawa, ON K1A 0H3, Canada.

[1]Corresponding author (e-mail: touzi@nrcan.gc.ca).

information from RADARSAT-1 SAR and Landsat VNIR data (Helie, 2004).

In this study, the use of the forthcoming Canadian RADARSAT-2 satellite is investigated for operational mapping and monitoring of Canadian wetlands. RADARSAT-2 will be the first satellite to carry a fully polarimetric C-band SAR while providing continuity of acquisition modes with RADARSAT-1. We have shown that the polarimetric information significantly improves the potential of C-band SAR for forest type discrimination (Touzi et al., 2004b). This should significantly improve wetland vegetation characterization and eventually bypass the use of weather-dependent VNIR satellite imagery for wetland mapping. The combination of RADARSAT-2 polarimetric and all-weather capabilities should provide unique information for operational mapping and monitoring of wetlands.

Polarimetric SARs have been investigated for wetland characterization (Pope et al., 1994; 1997; Hess et al., 1995; Sokol et al., 1998; 2004). The multipolarization information provided by the intensity of the HH, HV, and VV polarization is mainly investigated, and the HH–VV phase difference is used (Pope et al., 1994; Hess et al., 1995) for characterization of wetland target scattering in terms of odd- or even-bounce interactions (i.e., odd or even number of reflections; van Zyl, 1992). Target scattering decomposition has become the standard method for the extraction of natural target geophysical parameters from polarimetric SAR data (Boerner et al., 1998; Cloude and Pottier, 1996; Cloude and Pottier, 1997; van Zyl, 1992; Hajnsek et al., 2003; Touzi et al., 2004a). We show in this study that the application of target scattering decomposition on wetland leads to unique parameters that optimize the characterization of wetland classes.

The objective of the decomposition theory is to express the average target scattering mechanism as the sum of independent elements to associate a physical mechanism with each component (van Zyl, 1992; Cloude and Pottier, 1996). The Cloude–Pottier decomposition (Cloude and Pottier, 1996; 1997) has been currently the most used method for incoherent decomposition of natural extended target scattering. Recently, concerns have been raised regarding the Cloude α scattering type ambiguities that occur for certain scatterers (Corr and Rodrigues, 2002; Touzi, 2007), and a new method, the Touzi decomposition (Touzi, 2007), has been introduced for a roll and unique incoherent decomposition of target scattering. In contrast with the Cloude–Pottier decomposition, which characterizes target scattering type with a real entity, the so-called Cloude α, the Touzi decomposition uses the magnitude α_s and the phase ϕ_{α_s} of the "complex" symmetric scattering type introduced in Touzi (2007) for unambiguous characterization of target scattering. Target helicity (Kennaugh, 1951; Huynen, 1965) is used to assess the symmetric nature of target scattering. The new decomposition parameters should be worth investigating for wetland feature characterization, as demonstrated in this study.

The Touzi decomposition is briefly presented in the following section. The Mer Bleue wetland study site, which was surveyed by the Convair-580 polarimetric C-band SAR

(Livingstone et al., 1995), is described in a later section. The Touzi decomposition is applied to the polarimetric Convair-580 SAR data to derive roll-invariant wetland scattering parameters. In the last section, the Touzi decomposition parameters are analyzed with reference to ground measurements to assess the potential of the incoherent scattering decomposition for wetland class discrimination.

Touzi target decomposition in terms of roll-invariant target parameters

Like the Cloude–Pottier incoherent target decomposition (ICTD) (Cloude and Pottier, 1996), the Touzi decomposition (Touzi, 2007) is based on the incoherent characteristic decomposition of the coherency matrix [**T**]. For a reciprocal target, the characteristic decomposition of the Hermitian positive semidefinite target coherency matrix [**T**] permits the representation of [**T**] as the incoherent sum of up to three coherency matrices $[\mathbf{T}]_i$ representing three different single scatterers, each weighted by its appropriate positive real eigenvalue λ_i (Cloude, 1986):

$$[\mathbf{T}] = \sum_{i=1,3} \lambda_i [\mathbf{T}]_i \tag{1}$$

Each single scattering i ($i = 1, 3$) is represented by the coherency eigenvector matrix $[\mathbf{T}]_i$ of rank 1 and the corresponding normalized positive real eigenvalue $\lambda_i/(\lambda_1 + \lambda_2 + \lambda_3)$, which is a measure of the relative energy carried by the eigenvector i. In contrast with the Cloude–Pottier decomposition (Cloude and Pottier, 1996; 1997), the Touzi decomposition (Touzi, 2007) uses a roll-invariant coherent scattering model for the parameterization of the coherency eigenvectors in terms of unique target characteristics. Each coherent scatterer can be represented by the roll-invariant coherent scattering model given by (Touzi, 2007):

$$e_T^{SV} = m|e_T|_m \exp(j\phi_s)V \tag{2}$$

with

$$V = \begin{bmatrix} \cos\alpha_s \cos 2\tau_m \\ -j\cos\alpha_s \sin 2\psi \sin 2\tau_m + \cos 2\psi \sin\alpha_s \exp(j\phi_{\alpha_s}) \\ -j\cos\alpha_s \cos 2\psi \sin 2\tau_m + \sin 2\psi \sin\alpha_s \exp(j\phi_{\alpha_s}) \end{bmatrix} \tag{3}$$

For non-interferometric applications, the absolute target phase ϕ_s is ignored, and the coherent scatterer is uniquely characterized with five independents parameters, namely α_s, ϕ_{α_s}, ψ, τ_m, and m, where α_s and ϕ_{α_s} are the polar coordinates of the symmetric scattering type introduced in Touzi (2007); and ψ, τ_m, and m are the maximum polarization parameters (Kennaugh, 1951; Huynen, 1965; Boerner et al., 1991) (i.e., the orientation angle, helicity, and maximum return parameters, respectively).

Each coherency eigenvector i, which corresponds to a single scattering, is presented in terms of roll-invariant target scattering parameters as follows:

$$\text{ICTD}_i = (\lambda_i, m_i, \psi_i, \tau_{mi}, \alpha_{si}, \phi_{\alpha_s i}) \qquad (4)$$

Target scattering can be fully characterized by a deep analysis of each of the three eigenvector parameters of Equation (4). The normalized eigenvalues, which are identical to those generated by the Cloude–Pottier decomposition, may also be combined to derive the scattering entropy H and the anisotropy A introduced in Cloude and Pottier (1996; 1997) for the characterization of target scattering heterogeneity.

In this study, only the parameters α_s, ϕ_{α_s}, τ_m, λ, and H are investigated for wetland characterization. The maximum intensity m and the target tilt angle ψ will be considered in a future study. The new scattering type phase, ϕ_{α_s}, introduced in Touzi (2007) can only be exploited under coherence conditions. ϕ_{α_s} should be the most coherent (i.e., that corresponds to the highest coherence) for the dominant scattering, which is characterized with the coherency eigenvector of the highest eigenvalue λ_1 ($\lambda_1 > \lambda_2 > \lambda_3$). In the following, the dominant target scattering is investigated for wetland feature characterization. The coherence of the scattering type phase will be assessed using the degree of coherence introduced with the Touzi SSCM in Touzi and Charbonneau (2002). The information provided by λ_1, the entropy H, the symmetric scattering type magnitude and phase α_{s1} and $\phi_{\alpha_{s1}}$, and the target helicity τ_1 are analyzed with reference to ground measurements. In contrast with the partial information on single- or double-bounce interaction provided by the HH–VV phase difference investigated in Pope et al. (1994) and Hess et al. (1995), we should expect more valuable information from the Touzi decomposition parameters that fully characterize target scattering in a quantitative way.

Description of the Mer Bleue wetland study site and the data acquisition campaign

Mer Bleue Ramsar wetland study site

The Mer Bleue (45.30°N, 75.61°W) is a raised boreal peat dome located 10 km east of Ottawa, Canada. The site designated as a conservation area within the Greenbelt is protected by the National Capital Commission (NCC). The Mer Bleue Conservation Area was also designated as a Ramsar[2] wetland site in 1995. As part of its commitment under the Ramsar Convention by which Mer Bleue has been designated as a wetland of international importance, the NCC is interested in acquiring information and developing management tools that could help in the making of management decisions necessary to ensure the protection of the bog over the long term. This could involve assessing the ecological status of the wetland, monitoring environmental parameters and land use changes over time, and supporting scientific research and providing a better understanding of basic ecosystem functions. The NCC

has encouraged several studies on the Mer Bleue site to better understand the geological origins, palynology, and bog vegetation composition (Mott and Camfield, 1969; Belanger et al., 1977). In 1997–1998, the site was instrumented for peatland carbon research (fluxnet), and this led to the publication of several peer-reviewed papers related to the carbon budget (Moore et al., 2002; Bubier et al., 2003; 2006). The Mer Bleue site has also served as the basis for validation of remote sensing mapping approaches (Li and Chen, 2005; Baghdadi et al., 2001). The use of clear-sky-dependent Landsat appeared as a fundamental requirement for wetland vegetation characterization, since single-polarization RADARSAT has a poor potential for vegetation species discrimination (Toyra et al., 2001; Grenier et al., 2005; Toyra and Pietroniro, 2005). We show in this study that the additional polarimetric information provided by RADARSAT-2, and in particular the information related to the symmetric scattering type phase ϕ_{α_s}, permits an enhanced vegetation species discrimination and as such fills the gap related to single-polarization SAR. This may lead to an operational approach for wetland mapping and monitoring, which bypasses the use of weather-dependent VNIR satellite imagery, and as such is more suitable than the Landsat–RADARSAT approach for an updated CWI.

Data acquisition campaign

The Mer Bleue wetland site was surveyed by the Convair-580 polarimetric C-band SAR (Livingstone et al., 1995) in June 1995 at an illumination angle of about 55°. During the flight, corner and active reflectors were deployed for calibration, and aerial and ground photographs and in situ data have been collected to facilitate the identification of wetland classes and other surface types. The survey was done on 16 June, and the water level was high, with the last significant rainfall of 11.4 mm on 13 June.

Analysis of the Touzi decomposition parameters and discussions

Characterization of wetland classes

Mer Bleue wetland classes

The four main wetland classes present at Mer Bleue are marsh, treed bog, shrub bog, and fen. Theses classes are specified using the *Canadian Wetland Classification System* (National Wetlands Working Group, 1997). The shrub bog and fen are two similar and gradational environments; both are dominated by sphagnum moss and ericaceous shrubs, but the fen is richer in graminoides. The bog has a complete ground cover of sphagnum mosses with a shrub canopy dominated by ericaceous shrubs (Bubier et al., 2003). A secondary component of the community includes clusters of deciduous shrubs, discontinuous patches of black spruce and larch, and scattered sedges and cottongrass. Although most of the

---

[2] Intergovernmental convention on wetlands, signed in Ramsar, Iran, in 1971, for national action and international cooperation for the conservation and wise use of wetlands and their resources (www.ramsar.org).

peatland is composed of bog vegetation, there are also areas of poor fen. Poor fen vegetation is composed primarily of sedges and an understory of sphagnum mosses. The bog soils are rarely affected by the mineral-enriched groundwaters from surrounding soils, since precipitation, fog, and snow are the primary water sources. Marshes have persistent surface water underneath hygrophilous herbs (cattails). The borders of the bog form a typical lag environment that has been dammed by beaver, creating a zone of fluctuating water levels where marshes and ponds are found. Treed bog is mainly dominated by conifers (black spruce, tamarack, aspen, and pine). Upland areas mainly consist of deciduous-dominated forest and agriculture lands.

The aerial and ground photographs and in situ data collected during the flight have been combined with the Greenbelt forest cover inventory obtained from the NCC to identify the main wetland classes, as presented in **Figure 1**. The Greenbelt forest cover inventory layer is based on standard forest resources inventory methodologies current in Quebec and Ontario. The classification of **Figure 1** is used in the following section as the reference for the assessment and validation of the Touzi decomposition.

Analysis of the Touzi parameters for wetland classification

The Convair-580 polarimetric SAR data are processed, calibrated as described in Touzi et al. (2005), and then geocoded. **Figure 2** presents the HH-polarization image. For unbiased estimation of the Touzi decomposition parameters, we have shown (Touzi, 2007b) that the coherency matrix has to be estimated within a moving window that includes a minimum of 60 independent samples. The incoherent decomposition is applied on the Mer Bleue image with a moving window of approximately 60 independent looks. The dominant scattering parameters α_{s1}, $\phi_{\alpha_{s1}}$, $|\tau_1|$, and λ_1 are presented in **Figures 3, 4, 5, and 6**, respectively. **Table 1** summarizes the Touzi decomposition parameters estimated for the various classes within large windows presented in **Figure 2**; each window includes more than 1000 independent samples for accurate statistics.

To exploit $\phi_{\alpha_{s1}}$ information, $\phi_{\alpha_{s1}}$ should be coherent. As discussed in Touzi (2007), the complex symmetric scattering type phase and magnitude permit mapping each symmetric single scattering as a point on the surface of the symmetric scattering target Poincaré sphere (Touzi, 2002). Only a coherent symmetric scatterer can be represented as a point on the surface of the Poincaré sphere. A partially coherent
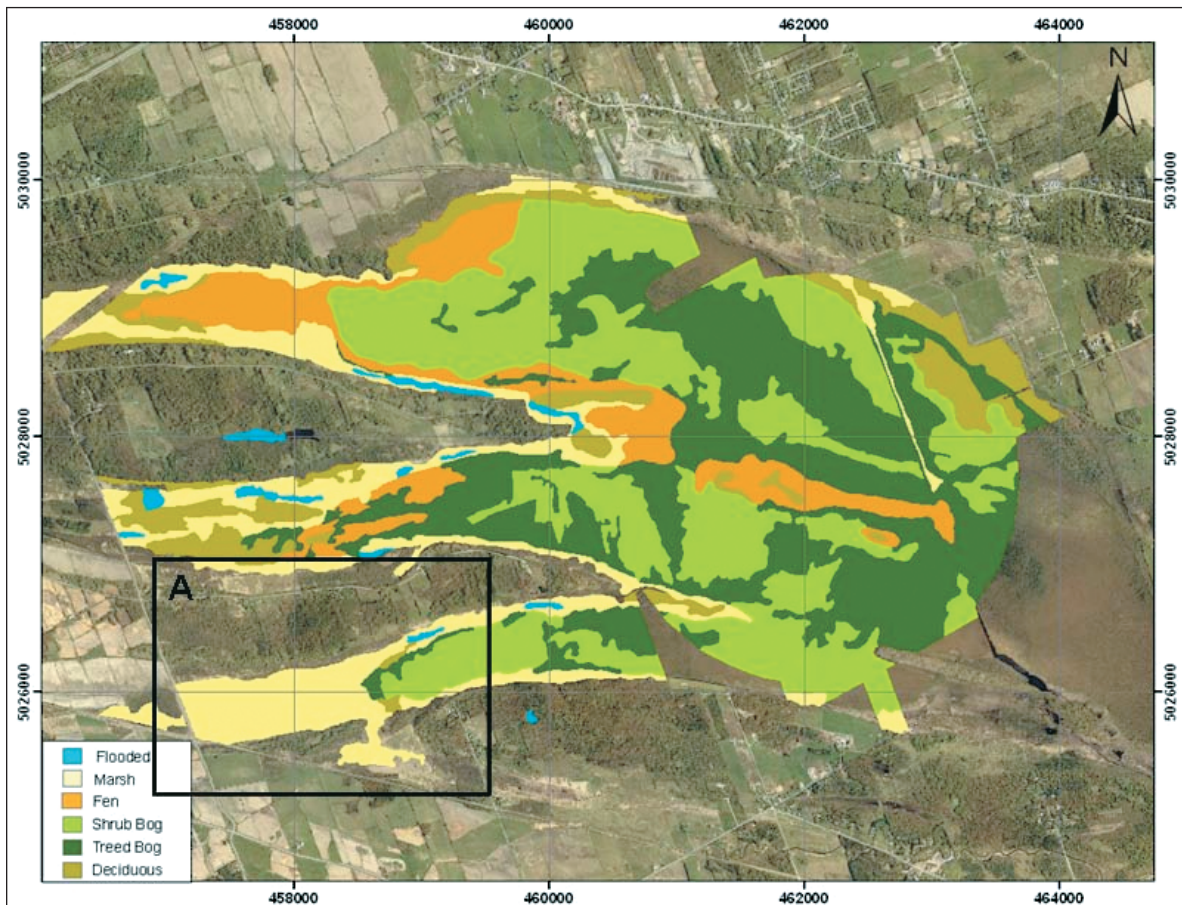
Figure 1. Wetland classification based on the forest inventory provided by the National Capital Commission (NCC). Grid coordinates are UTM Zone 18 eastings and northings based on the WGS84 ellipsoid. A, subset presented in **Figures 8–10**.
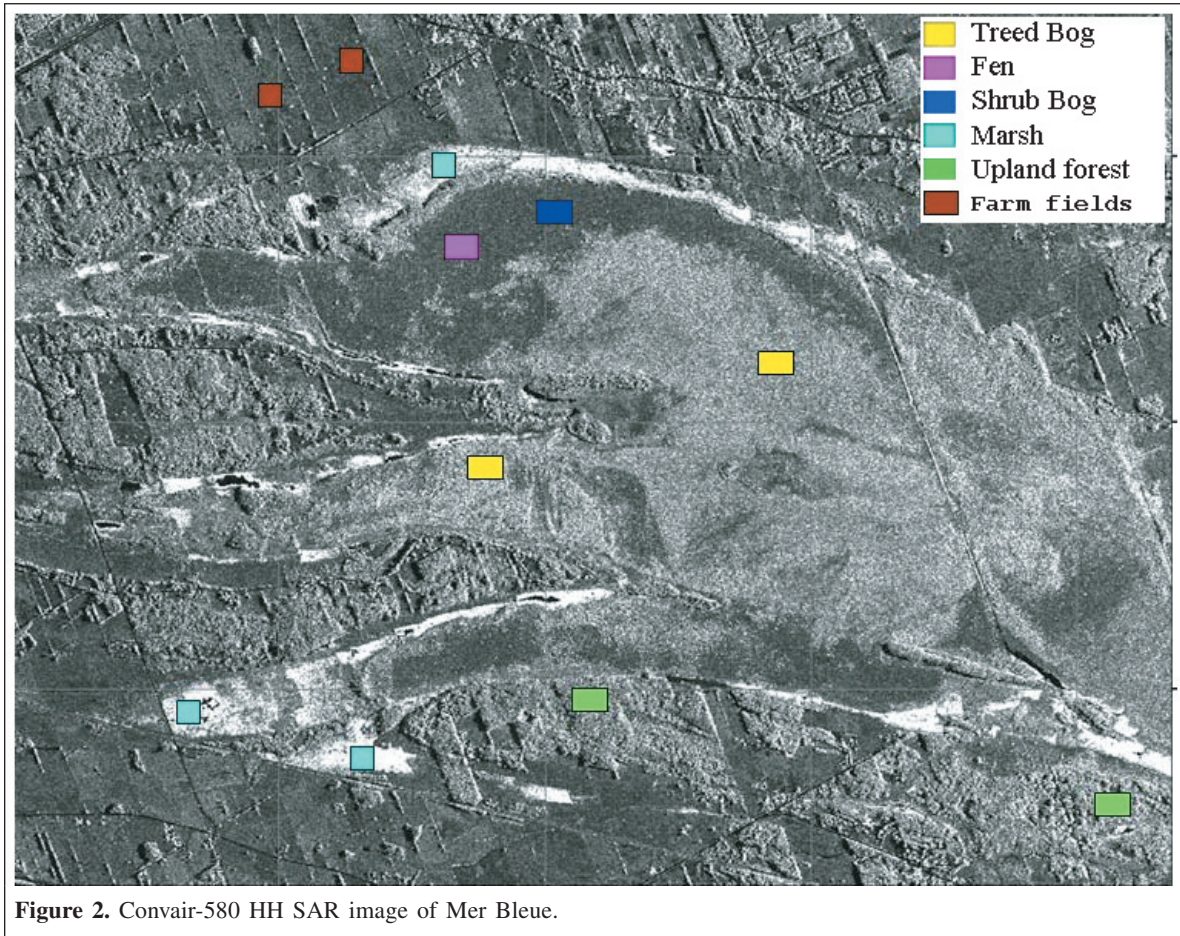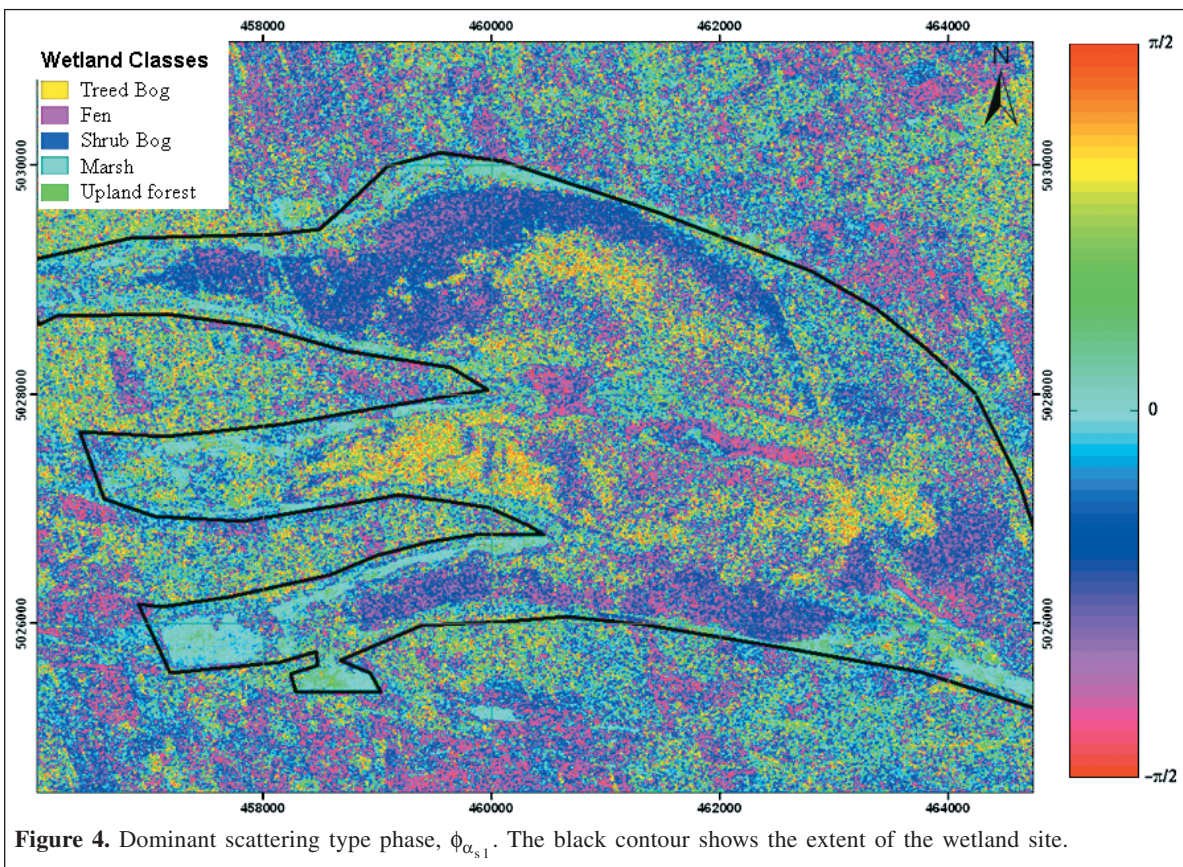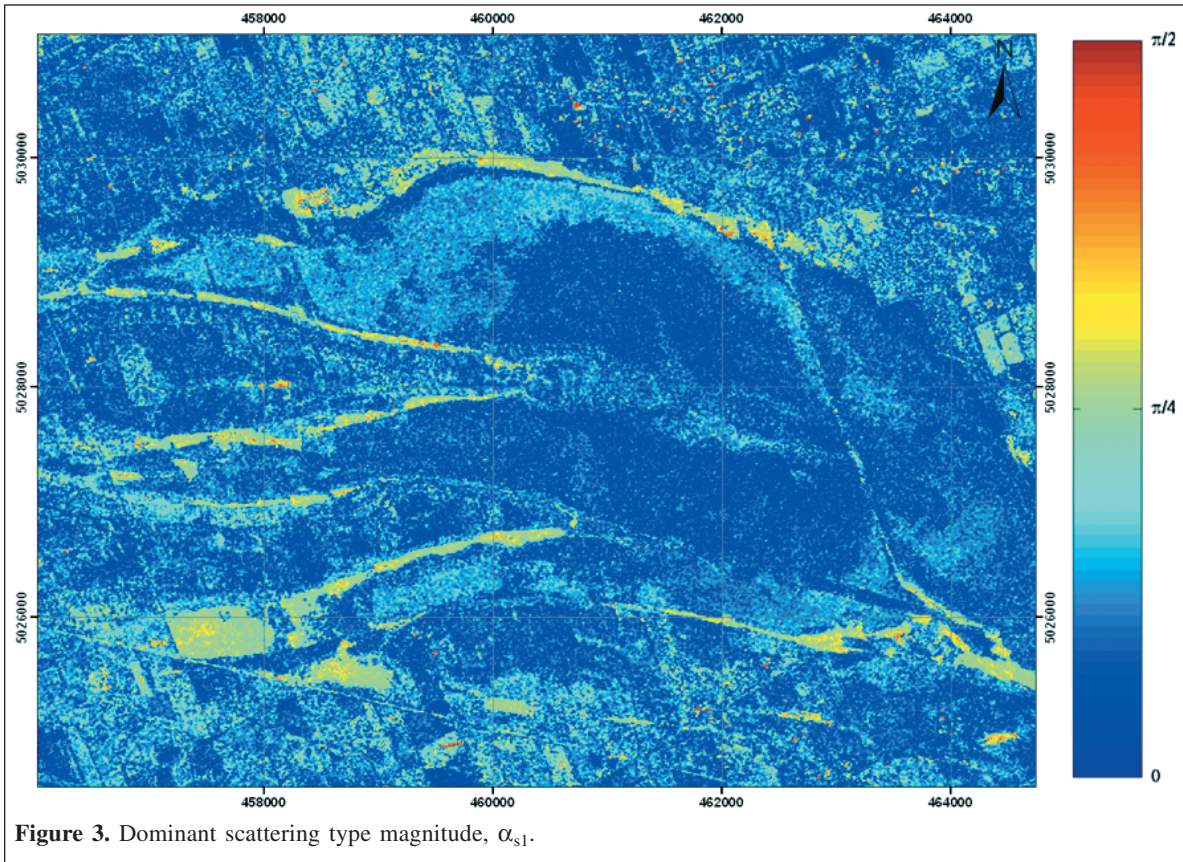
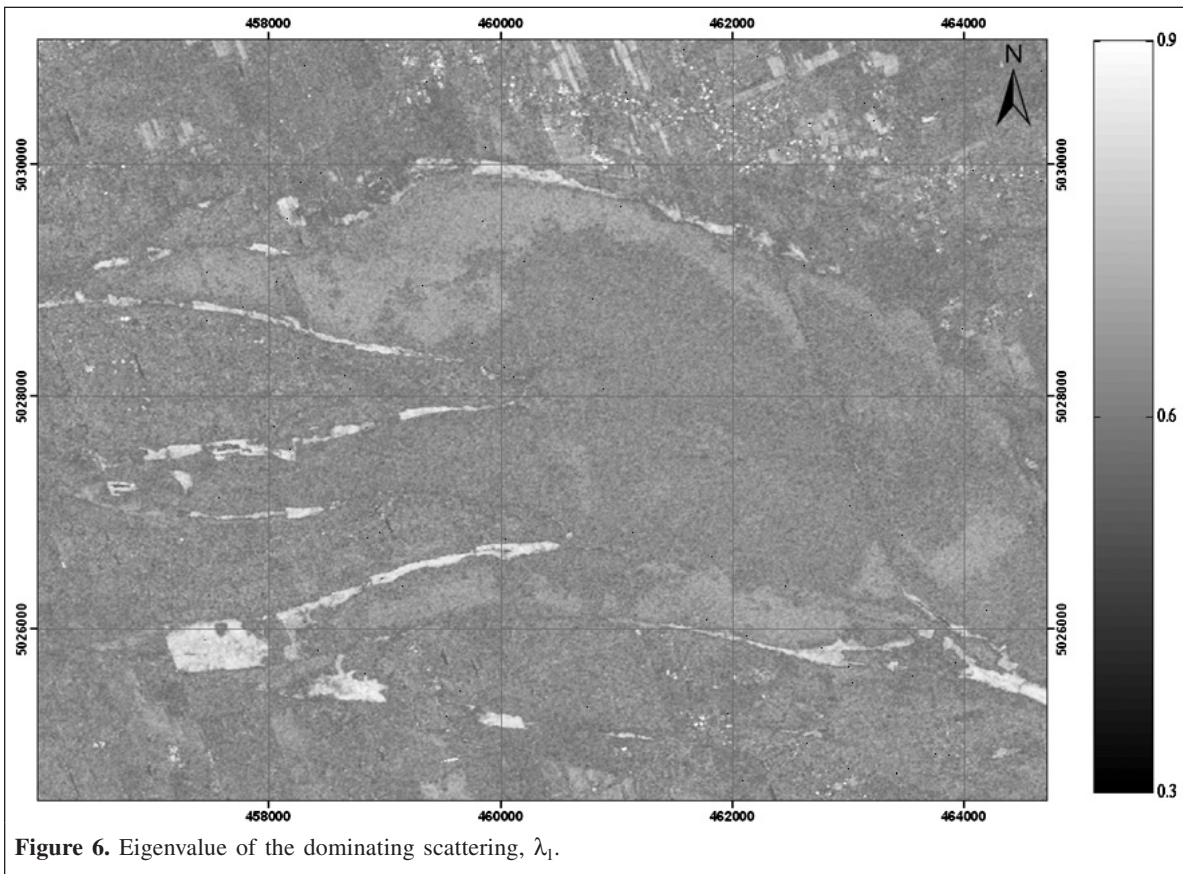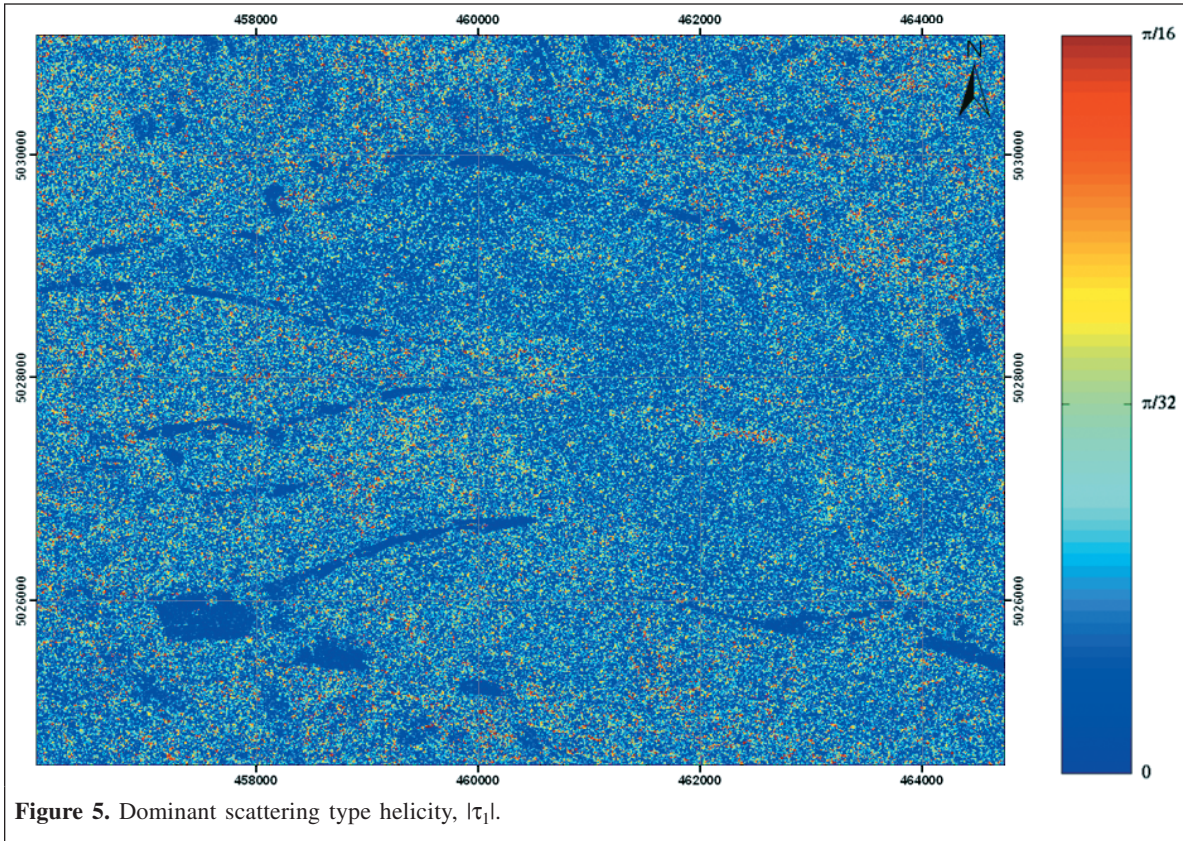**Figure 2.** Convair-580 HH SAR image of Mer Bleue.

symmetric scatterer is represented as a point inside the sphere at a distance from the sphere centre determined by the degree of coherence introduced in Touzi and Charbonneau (2002). In contrast with the Cameron disc representation (Cameron et al., 1996), which is limited to the coherent scattering, the Poincaré sphere representation permits characterization of both coherent and partially coherent scattering. To assess the coherence of $\phi_{\alpha_{s1}}$, its degree of coherence $p_{\phi_{\alpha_{s1}}}$ is computed and presented in **Figure 7**. For a completely coherent scatterer, $p_{\phi_{\alpha_{s1}}} = 1$ and the scatterer is on the surface of the Poincaré sphere. The main advantage of the use of $p_{\phi_{\alpha_{s1}}}$ in comparison with the conventional coherence (Touzi et al., 1999), is that the coherence remains high even when the symmetric signal energy is carried by only one channel (trihedral or dihedral scattering) in the trihedral–dihedral symmetric scattering decomposition (Touzi and Charbonneau, 2002). The analysis of the $p_{\phi_{\alpha_{s1}}}$ image of **Figure 7** leads to the following conclusion: $\phi_{\alpha_{s1}}$ is highly coherent within the wetland site delineated in **Figure 4**, with a degree of coherence $p_{\phi_{\alpha_{s1}}}$ higher than 0.85. With λ_1 generally larger than 0.60 inside the wetland site, as seen in **Figure 6**, the wetland target energy carried by the dominant scattering remains sufficiently high, and this leads to a sufficiently high coherent phase $\phi_{\alpha_{s1}}$ that can be efficiently exploited for wetland characterization. The potential of the

dominant scattering parameters α_{s1}, $\phi_{\alpha_{s1}}$, and $|\tau_1|$ is discussed in the following.

As presented in **Figure 5**, $|\tau_1|$ indicates the degree of symmetry of wetland scattering: the higher the value of $|\tau_1|$, the more asymmetric the scattering. As can be seen in **Figure 5** and **Table 1**, with the exception of treed bog and uplands forests that have a significant helicity value, wetland classes identified in **Figure 1** are dominated by symmetric scattering with $|\tau_1|$ values lower than 10°. For theses symmetric targets, the symmetric scattering type magnitude and the Cloude scattering type are similar: $\alpha_{s1} \simeq \alpha_1$. We show in the following that α_{s1} (and as such $\alpha_1 \simeq \alpha_{s1}$) is not efficient for wetland classification. The new symmetric scattering type phase $\phi_{\alpha_{s1}}$ introduced in Touzi (2007) provides the missing key information for vegetation type discrimination, and this leads to a significant improvement in wetland classification.

The analysis of the symmetric scattering type magnitude α_{s1} of **Figure 3**, which is identical to the Cloude α_1 for most wetland classes, reveals that both α_{s1} and α_1 are not efficient for wetland class discrimination. The poor potential of α_1 and α_{s1} in vegetation species discrimination confirms the limitation of the scattering type radiometric information for wetland classification. Even combined with the entropy H, α_1 and α_{s1} lead to a classification very similar to that of the single-
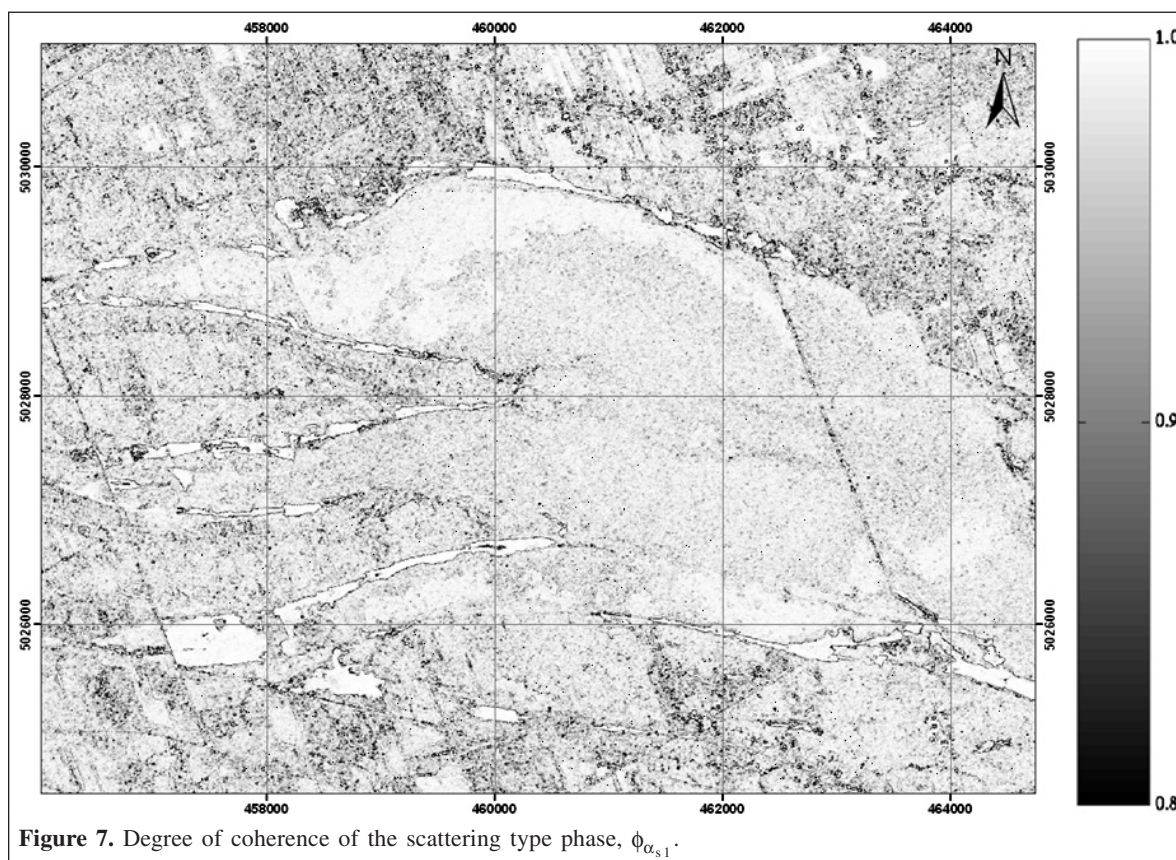
Figure 3. Dominant scattering type magnitude, α_{s1}.

Figure 4. Dominant scattering type phase, $\phi_{\alpha_{s1}}$. The black contour shows the extent of the wetland site.

Figure 5. Dominant scattering type helicity, $|\tau_1|$.

Figure 6. Eigenvalue of the dominating scattering, λ_1.

Figure 7. Degree of coherence of the scattering type phase, $\phi_{\alpha_{s1}}$.

Table 1. Decomposition parameters of representative samples.

Class	HH (dB)	α_{s1} (°)	$\phi_{\alpha_{s1}}$ (°)	$|\tau_1|$ (°)	λ_1	Entropy
Marsh	−5.2	45.3	1.40	0.5	0.92	0.31
Sedge fen	−16.6	24.5	−38.10	4.5	0.66	0.79
Shrub bog	−16.3	25.8	−56.40	5.2	0.64	0.81
Conifer treed bog	−11.5	20.9	49.27	19.3	0.57	0.89
Upland deciduous forest	−12.8	18.4	22.80	16.6	0.58	0.88
Agriculture fields	−16.1	15.3	−29.80	9.6	0.55	0.80

polarization HH. Three major classes can be discriminated using HH or the scattering type entropy information. The marsh class of very high return at the HH polarization, with a scattering coefficient $\sigma^0 = -5.2°$ dB in **Table 1**, appears very bright in the HH image of **Figure 2** and in green in the α_{s1} image of **Figure 3**. Marsh acts as a pure and low-entropy dipole scattering with $\alpha_{s1} \approx 45°$, $\lambda_1 = 0.92$, and $H = 0.31$ in **Table 1**. The second class (dark in HH of **Figure 2**, with $\sigma^0 \approx -16$ dB in **Table 1**, and light blue in **Figure 3**) corresponds to the so-called medium-entropy surface scattering class of Cloude and Pottier (1997), with a high entropy ($H = 0.79$ in **Table 1**).[3] This class regroups farm fields, sedge (dominated) fen, sedge (dominated) bogs, and shrub (dominated) bogs. The third class (grey in HH of **Figure 2**, with $\sigma^0 \approx -12$ dB in **Table 1**, and blue

in **Figure 3**) regroups conifer (dominated) treed bogs and upland deciduous forests. Their scattering can be assigned to the high-entropy surface scattering class of Cloude and Pottier (1997), with α_{s1} of about 20° (α_1 about 43°) and a very high entropy (about 0.88), as seen in **Table 1**. This class was qualified in Cloude and Pottier (1997) as "not exploitable" from the polarimetric point of view because of the scattering type (α_1 and α_{s1}) ambiguity due to the very high entropy. Similar to the Cloude α_1, the high entropy value limits the α_{s1} capability for the discrimination of conifer (dominated) treed bogs from upland deciduous forests. The helicity τ_1, which solves for the α ambiguity related to target asymmetry, cannot discriminate these targets of high-entropy scattering. We see in the following that such an ambiguity can be solved by the

[3] Note that the Cloude–Pottier $\alpha|H$ classification of Cloude and Pottier (1997) is obtained with the scattering type of the "average" scattering. The same method can be extended to the dominant scattering type, as done here.

additional phase information $\phi_{\alpha_{s1}}$, which permits taking full advantage of the polarimetric SAR information for better characterization of wetland targets.

The results obtained previously with the scattering type combined with entropy show that the fully polarimetric capability of RADARSAT-2 may not provide superior classification compared with that from the single HH RADARSAT-1 polarization. Like HH RADARSAT-1, the poor potential of the scattering type radiometric information for vegetation species discrimination may not permit the use of RADARSAT-2 as sole source for wetland classification, and Landsat may be required for improved wetland vegetation discrimination. The results obtained here regarding the scattering type radiometry inefficiency in vegetation species discrimination are in agreement with those from previous studies (Touzi et al., 2004b) in which we demonstrated that the Cloude α (and as such α_s, which is identical to α for symmetric scattering) is not effective for forest type discrimination, even when combined with the entropy H. We show in the following that the phase $\phi_{\alpha_{s1}}$ of the symmetric scattering type provides the key information missed by α_{s1} and α_1 for an enhanced vegetation type discrimination, and this leads to more effective wetland classification. This should promote the use of the fully polarimetric all-weather RADARSAT-2 as the sole source of information for wetland mapping and monitoring.

In **Figure 4**, a colour wheel with equally spaced bins between $-\pi/2$ and $\pi/2$ is used to represent the symmetric scattering type phase $\phi_{\alpha_{s1}}$. The wetland site is identified in **Figure 4** with the black contour, which separates the wetland site from upland areas. Even though no $\phi_{\alpha_{s1}}$-based classification process has been applied, the four wetland classes identified in **Figure 1** are well discriminated with $\phi_{\alpha_{s1}}$ in **Figure 4**: marsh (turquoise), treed bog (yellow), shrub bog (dark blue), and fen (magenta). The phase $\phi_{\alpha_{s1}}$ can separate well (about 25° offset according to **Table 1**) the treed bog dominated by conifers (mainly black spruce) from the upland forest dominated mainly by deciduous trees (poplar, maple, and willow) and can also discriminate sedge-dominated fens from shrub-dominated bogs, with about 20° phase offset between the two classes according to **Table 1** and **Figure 4**.

The results obtained with $\phi_{\alpha_{s1}}$ within the wetland site looks very promising. However, discrimination of wetland classes from upland areas looks less efficient, as seen in **Figure 4**. Although $\phi_{\alpha_{s1}}$ permits good separation of sedge fen from shrub bog, it cannot discriminate sedge fen from agriculture fields, as seen in **Figure 4** and **Table 1**. These two targets may be better discriminated using the degree of coherence image $p_{\phi_{\alpha_{s1}}}$ of **Figure 7**, in which the agriculture fields demonstrate lower phase coherence than fens. Enhanced discrimination can be obtained using the dominant scattering eigenvalue λ_1 of **Figure 6**. Like the entropy H, λ_1 permits assessment of the dominant scattering homogeneity, with the highest value (i.e., 1) for a pure single scattering (of entropy zero). The analysis of **Figure 6** and **Table 1** leads to the conclusion that fen scattering is more homogeneous (i.e., pure) than agriculture field scattering; $\lambda_1 \simeq 0.66$ for sedge fen, whereas $\lambda_1 \simeq 0.55$ for

agriculture fields. This may be explained by the presence of the water underneath the vegetation that minimizes the volume-scattering component. As a result, the coherence $p_{\phi_{\alpha_{s1}}}$ of sedge fen is much higher than that of agriculture fields, as seen in **Figure 7**. The combination of $\phi_{\alpha_{s1}}$ with λ_1 or $p_{\phi_{\alpha_{s1}}}$ permits better discrimination of the sedge fen from agriculture fields and should lead to a more effective wetland classification. Notice also for the marsh class that the high surface water level underneath cattails leads to more pure scattering (low entropy) with a high value of $\lambda_1 \simeq 0.90$, as seen in **Figure 6**.

Characterization of target scattering

Even though $\phi_{\alpha_{s1}}$ permits better wetland class discrimination than the magnitude of the scattering type magnitude α_{s1}, both phase and magnitude of the complex symmetric scattering type are needed for unambiguous characterization of symmetric target scattering (Touzi, 2007). **Figure 8** is an aerial photograph of the subset shown in **Figure 1**, and **Figures 9** and **10** show the same area and present the dominant scattering type magnitude and phase, α_{s1} and $\phi_{\alpha_{s1}}$. The marshes are well identified in the α_{s1} and $\phi_{\alpha_{s1}}$ images as green–yellow in α_{s1} of **Figure 9** and turquoise–green in $\phi_{\alpha_{s1}}$ of **Figure 10**. The part within the marsh field that looks green in **Figure 9** and turquoise–green in **Figure 10** corresponds to a dipole scattering (i.e., horizontal thin cylinder) with $\alpha_{s1} = 45°$ and $\phi_{\alpha_{s1}} = 0$ (Touzi, 2007). Such a scattering of low entropy (H about 0.3 in **Table 1**) may result from the sum of two equally weighted single scatterings, the trihedral and dihedral scattering (i.e., first and second Pauli matrix (Touzi, 2007)). The trihedral scattering is due to direct scattering from cattails, or tri-bounce cattail–water–cattail reflections. The dihedral is due to the wave interactions of water–cattail. Notice that for more spaced cattails (open cattails indicated by the arrow), the cattail–water–cattail interactions are reduced and the dihedral scattering becomes dominant (yellow in **Figure 9**). These two different scattering mechanisms would be assigned to the same mechanism, the double-bounce scattering, if the phase difference between HH and VV (van Zyl, 1989) were used for scattering identification, as done in Pope et al. (1994; 1997) and Hess et al. (1995). It is also worth noting in **Figure 9** that the pure dihedral scattering (red in **Figure 9**) on the borders of open-water areas is easily identified in **Figure 8**. These two examples bring out the high potential of the symmetric scattering type magnitude and phase for target scattering identification in comparison with the HH–VV phase difference method, which uses a very simplified representation of scattering type in terms of odd- and even-bounce dominant scattering components.

Conclusion

This study investigated target scattering decomposition for wetland classification. The Touzi decomposition, which permits a roll-invariant target scattering decomposition, leads to the characterization of wetland classes in terms of unique

Figure 8. Aerial photograph of subset A from **Figure 1**. The arrow shows an open cattails area.
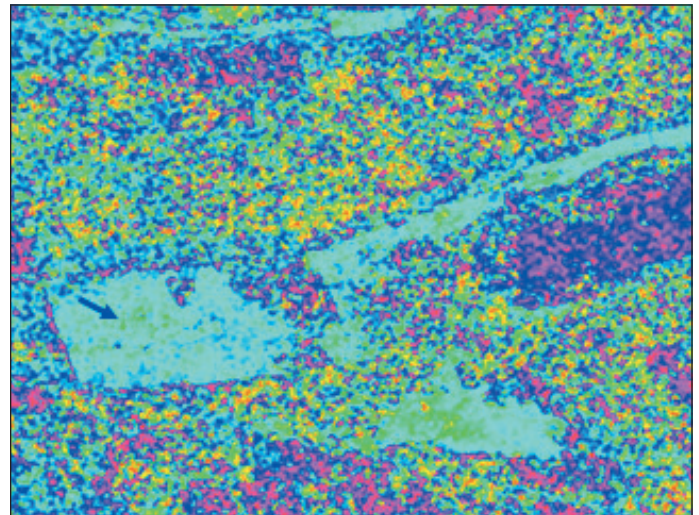
Figure 10. Subset dominant scattering type phase, $\phi_{\alpha_{s1}}$. Arrow as in **Figure 8**.
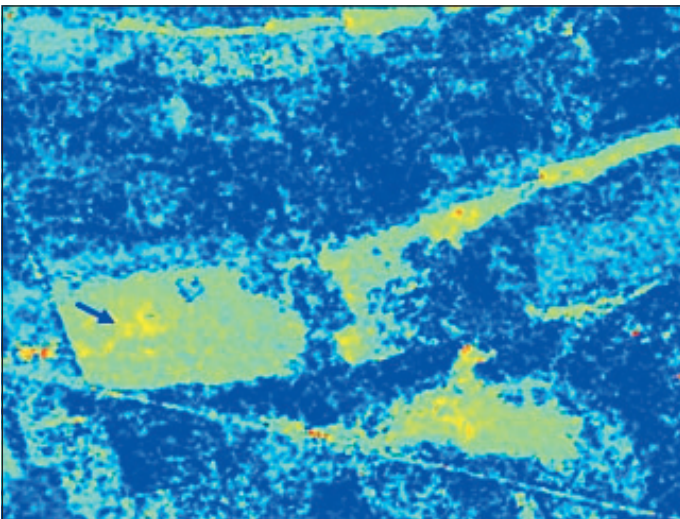
Figure 9. Subset dominant scattering type magnitude, α_{s1}. Arrow as in **Figure 8**.

target parameters: the symmetric scattering type magnitude and phase, α_s and ϕ_{α_s}, and the target helicity, τ_m, for assessment of target scattering symmetry. It is shown that the scattering type radiometric information, which is provided by α_s or the Cloude α combined with the entropy H, does not permit taking full advantage of polarimetric SAR for an effective wetland classification. As with HH RADARSAT-1, the poor potential of α_s and α for discrimination of wetland vegetation species limits the efficiency of polarimetic SAR for wetland classification. The new phase $\phi_{\alpha_{s1}}$ of the symmetric scattering type introduced in Touzi (2007) provides the key information missed by α_{s1} and α_1 for an enhanced vegetation type discrimination, and this leads to more effective wetland classification. The use of the dominant scattering type phase, $\phi_{\alpha_{s1}}$, makes possible the discrimination of shrub-dominated bog from sedge-dominated fen and even

permits the discrimination of conifer-dominated treed bog from upland deciduous forest under leafy conditions. The new phase $\phi_{\alpha_{s1}}$ permits a clear identification of the four Mer Bleue wetland classes: sedge fen, marsh, shrub bog, and conifer-dominated treed bog. The combination of $\phi_{\alpha_{s1}}$ with λ_1 or the coherence p_{sym} should enhance the discrimination between the sedge-dominated fen and agricultural fields, and as such should improve wetland classification. However, the use of the scattering type magnitude α_s in addition to the phase information ϕ_{α_s} remains essential for an unambiguous description of wetland target scattering.

In this study, we have emphasized the importance of the phase of the dominant scattering type for wetland characterization. Better results should be obtained if the parameters of the second and the lowest scattering components are also considered. In the future, all the parameters derived from the decomposition of the three coherency eigenvectors will be considered. The Touzi decomposition parameters will be combined with the Cloude–Pottier entropy and anisotropy and used as the basis for the development of a unique wetland classification method, which should optimize the exploitation of RADARSAT-2 polarimetric information for wetland characterization. Further investigations are currently being conducted, in collaboration with the Canadian Wildlife Service of Environment Canada and Parks Canada, on other types of wetlands to confirm the high potential of polarimetric RADARSAT-2 for wetland classification and the possibility of using the all-weather polarimetric RADARSAT-2 as the sole source of information for wetland mapping and monitoring in the Canadian Wetland Inventory (CWI).

Acknowledgements

References

Baghdadi, N., Bernier, M., Gauthier, R., and Nesson, I. 2001. Evaluation of C-band SAR data for wetlands mapping. *International Journal of Remote Sensing*, Vol. 22, No. 1, pp. 71–88.

Belanger, J.R., and Harrison, J.E. 1977. *Bedrock geology, drift thickness trend, and bedrock topography, Ottawa–Hull, Ontario and Quebec*. Geological Survey of Canada, Paper 77-11. 18 pp.

Boerner, W.M., Yan, W.-L., Xi, A.-Q., and Yamaguchi, Y. 1991. On the principles of radar polarimetry (invited review): the target characteristic polarization state theory of Kennaugh, Huynen's polarization fork concept, and its extension to the partially polarized case. *IEEE Proceedings, Special Issue on Electromagnetic Theory*, Vol. 79, No. 10, pp. 1538–1550.

Boerner, W.M., Mott, H., Lüneburg, E., Livingstone, C., Brisco, B., Brown, R.J., Paterson, J.S., Cloude, S.R., Krogager, E., Lee, J.S., Schuler, D.L., Van Zyl, J.J., Randall, D., Budkewitsch, P., and Pottier, E. 1998. Polarimetry in radar remote sensing: basic and applied concepts. In *Manual of remote sensing: principles and applications of imaging radar*. Edited by R.A. Ryerson. John Wiley & Sons, Inc., New York. Vol. 3, No. 5, pp. 271–356.

Bubier, J.L., Bhatia, G., Moore, T.R., Roulet, N.T., and Lafleur, P.M. 2003. Between year and site variability in growing season net ecosystem CO2 exchange controlled by respiration at a large peatland, Ontario, Canada. *Ecosystems*, Vol. 6, pp. 353–365.

Bubier, J.L., Moore, T.R., and Crosby, T.R. 2006. Fine-scale vegetation distribution in a cool temperate peatland. *Canadian Journal of Botany*, Vol. 84, pp. 910–923.

Cameron, W.L., Youssef, N., and Leung, L.K. 1996. Simulated polarimetric signatures of primitive geometrical shapes. *IEEE Transactions on Geoscience and Remote Sensing*, Vol. 34, No. 3, pp. 793–803.

Cloude, S.R. 1986. Group theory and polarization algebra. *Optik*, Vol. 75, No. 1, pp. 26–36.

Cloude, S.R., and Pottier, E. 1996. A review of target decomposition theorems in radar polarimetry. *IEEE Transactions on Geoscience and Remote Sensing*, Vol. 34, No. 2, pp. 498–518.

Cloude, S.R., and Pottier, E. 1997. An entropy based classification scheme for land applications of polarimetric SARs. *IEEE Transactions on Geoscience and Remote Sensing*, Vol. 35, No. 2, pp. 68–78.

Corr, D.G., and Rodrigues, A.F. 2002. Alternative basis matrices for polarimetric decomposition. In *EUSAR 2002, Proceedings of the 4th European Union Conference on Synthetic Aperture Radar*, 4–6 June 2002, Cologne, Germany.

Grenier, M., Dermers, A.M., Labrecque, S., Fournier, R., Drolet, B., and Benoit, M. 2005. La cartographie des terres humides au Québec dans le cadre de l'inventaire canadien des terres humides: Approche m'ethodologique. In *Proceedings of the 12th Congress of l'Association Quebébécoise de Télédétection*, May 2005, Chicoutimi, Que. CD-ROM. Edited by Y. Gauthier and D. Haboudane. L'Association Quebébécoise de Télédétection (AQT), Sainte-Foy, Que.

Hajnsek, I., Pottier, E., and Cloude, S.R. 2003. Inversion of surface parameters from polarimetric SAR. *IEEE Transactions on Geoscience and Remote Sensing*, Vol. 41, No. 4, pp. 727–744.

Helie, R. 2004. *Canadian Wetland Inventory*. Available from www.wetkit.net/modules/4/index.php.

Hess, L.L., Melack, J.M., Filoso, S., and Wang, Y. 1995. Delineation of inundated areas and vegetation along the Amazon floodplain with SIR-C synthetic aperture radar. *IEEE Transactions on Geoscience and Remote Sensing*, Vol. 33, No. 4, pp. 896–904.

Huynen, J.R. 1965. Measurement of the target scattering matrix. *Proceedings of IEEE*, Vol. 53, No. 8, pp. 936–946.

Ito, N., Hamazaki, T., and Tomioka, K. 2001. ALOS/PALSAR characteristics and status. In *Proceedings of the CEOS SAR Workshop 2001*, 2–4 April 2001, Tokyo. National Space Development Agency of Japan (NASDA), Tokyo. pp. 191–194.

Kennaugh, K. 1951. *Effects of type of polarization on echo characteristics*. Antenna Laboratory, Ohio State University, Columbus, Ohio. Technical Reports 389-4 (35 pp.) and 381-9 (39 pp.).

Li, J., and Chen, W. 2005. A rule-based method for mapping Canada's wetland using optical, radar and DEM data. *International Journal of Remote Sensing*, Vol. 26, No. 22, pp. 5051–5069.

Livingstone, C.E., Gray, A.L., Hawkins, R.K., Vachon, P.W., Lukowski, T.I., and LaLonde, M. 1995. The CCRS airborne SAR systems: radar for remote sensing research. *Canadian Journal of Remote Sensing*, Vol. 21, No. 4, pp. 468–491.

Moore, T.R., Bubier, J.L., Frolking, S.E., Lafleur, P.M., and Roulet, N.T. 2002. Plant biomass and production and CO2 exchange in an ombrotrophic bog. *Journal of Ecology*, Vol. 90, No. 1, pp. 25–36.

Mott, R.J., and Camfield, M. 1969. *Palynological studies in the Ottawa area*. Geological Survey of Canada, Paper 69-38. 16 pp.

National Wetlands Working Group. 1997. *Canadian Wetland Classification System*. 2nd ed. Edited by B.G. Warner and C.D.A. Rubec. Wetlands Research Centre, University of Waterloo, Waterloo, Ont. 68 pp.

Pope, K.O., Rey-Benays, J.M., and Paris, J.F. 1994. Radar remote sensing of forest and wetland ecosystems in the Central American tropics. *Remote Sensing of Environment*, Vol. 48, pp. 205–219.

Pope, K.O., Rejmankova, E., Paris, J.F., and Woodruff, R. 1997. Detecting seasonal flooding cycles in marches of the Yucatan Peninsula with SIR-C polarimetric radar imagery. *Remote Sensing of Environment*, Vol. 59, pp. 157–166.

Sokol, J., McNairn, H., Pultz, T., Touzi, R., and Livingstone, C. 1998. Monitoring wetland hydrology with airborne polarimetric radar. In *Proceedings of the 20th Canadian Symposium on Remote Sensing*, 25–30 May 1998, Calgary, Alta. Canadian Aeronautics and Space Institute, Ottawa, Ont.

Sokol, J., McNairn, H., and Pultz, T.J. 2004. Case studies demonstrating the hydrological applications of C-band multipolarized and polarimetric SAR. *Canadian Journal of Remote Sensing*, Vol. 30, No. 3, pp. 470–483.

Touzi, R. 2007a. Speckle effect on polarimetric target scattering decomposition of SAR imagery. *Canadian Journal of Remote Sensing*, Vol. 33, No. 1, pp. 60–68.

Touzi, R. 2007b. Target scattering decomposition in terms of roll invariant target parameters. *IEEE Transactions on Geoscience and Remote Sensing*, Vol. 45, No. 1, pp. 73–84.

Touzi, R., and Charbonneau, F. 2002. Characterization of target symmetric scattering using polarimetric SARs. *IEEE Transactions on Geoscience and Remote Sensing*, Vol. 40, pp. 2507–2516.

Touzi, R., Lopes, A., Bruniquel, J., and Vachon, P.W. 1999. Coherence estimation for SAR imagery. *IEEE Transactions on Geoscience and Remote Sensing*, Vol. 37, pp. 135–149.

Touzi, R., Boerner, W.M., Lee, J.S., and Lueneburg, E. 2004a. A review of polarimetry in the context of synthetic aperture radar: concepts and information extraction. *Canadian Journal of Remote Sensing*, Vol. 30, No. 3, pp. 380–407.

Touzi, R., Landry, R., and Charbonneau, F.J. 2004b. Forest type discrimination using calibrated C-band polarimetric SAR data. *Canadian Journal of Remote Sensing*, Vol. 30, No. 3, pp. 543–551.

Touzi, R., Livingstone, C.E., and Charbonneau, F. 2005. A general method for calibration of the C-band Convair-580 SAR. *Canadian Journal of Remote Sensing*, Vol. 31, No. 1, pp. 52–60.

Toyra, J., and Pietroniro, A. 2005. Towards operational monitoring of a northern wetland using geomatics-based techniques. *Remote Sensing of Environment*, Vol. 97, pp. 174–191.

Toyra, J., Pietroniro, A., and Martz, L. 2001. Multisensor hydrologic assessment of a freshwater wetland. *Remote Sensing of Environment*, Vol. 75, pp. 162–173.

van Zyl, J.J. 1989. Unsupervised classification of scattering behavior using radar polarimetry data. *IEEE Transactions on Geoscience and Remote Sensing*, Vol. 27, No. 1, pp. 37–45.

van Zyl, J.J. 1992. Application of Cloude's target decomposition theorem to polarimetric imaging radar data. In *Radar polarimetry*. Edited by H. Mott and W.-M. Boerner. International Society for Optical Engineering, Bellingham, Wash. Proceedings of SPIE Vol. 1748, pp. 184–191.